

## An Integrated Hybrid Power System Based on Solar PV Array and Wind Turbine Doubly Fed Induction Generator for Basrah, Iraq

Ban Hamdan<sup>1</sup>, Naqui Anwer<sup>2</sup>

Senior Engineer, Iraqi Port Company, Iraq  
Research Scholar, Jamia Millia Islamia, New Delhi, India

### ABSTRACT

*Non conventional or Renewable energy sources fetch wide attention in the last two decades due to persisting energy demand and decrease in petroleum resources and its environmental effect to the earth. In Iraq, the electric power generated is not enough to meet the power demand of domestic and industrial sectors. In this research paper, a hybrid system was proposed based on Solar Photovoltaic Array (SPA) and Wind Turbine Doubly Fed Induction Generator (WTDFIG) as a renewable resource of power generation for grid connected applications in the city of Basrah, Iraq. The proposed system has been simulated using MATLAB (version R2011a). The models are first made to run as standalone systems and then as integrated model in which the input parameters are the average monthly meteorological data for the city of Basrah, Iraq. Results showed that it is possible for Iraq to use the solar and wind energy to generate enough power for the city under consideration. It is also possible to use such a system as a source of power during total shutdown time for any villages in the desert or rural area.*

**Keywords:** Solar Photovoltaic Array, Wind Turbine, SPA, WTDGFIG, MATLAB, Basrah

### 1. INTRODUCTION

For the appropriate results obtained from the models, it is necessary to develop the models based on the conceptual basic equations for solar as well as wind turbine based generation. This section will elaborate the design and simulation aspects of the

standalone and integrated models of SPA and WTDFIG.

### 1.1 MODELLING AND SIMULATION OF SPA

PV arrays are built up with combined series/parallel combinations of PV solar cells, which are usually represented by a simplified equivalent circuit model such as the one given in Fig. 1 and/or by an equation as in (3.1).

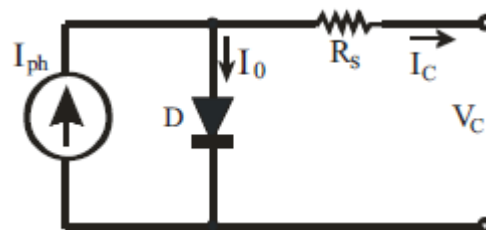


Fig. 1 Simplified Equivalent Circuit of Photovoltaic Cell.

The PV cell output voltage is a function of the photocurrent that mainly determined by load current depending on the solar irradiation level during the operation.

$$V_c = \frac{AkT_c}{e} \ln \left( \frac{I_{ph} + I_0 - I_c}{I_0} \right) - R_s I_c \quad 1.1$$

Where the symbols are defined as follows:

e: electron charge ( $1.602 \times 10^{-19}$  C).

k: Boltzmann constant ( $1.38 \times 10^{-23}$  J/°K).

I<sub>c</sub>: cell output current, A.

I<sub>ph</sub>: photocurrent, function of irradiation level and junction temperature (5 A).

I<sub>0</sub>: reverse saturation current of diode (0.0002 A).

R<sub>s</sub>: series resistance of cell (0.001 Ω).

T<sub>c</sub>: reference cell operating temp (20 °C).

V<sub>c</sub>: cell output voltage, V.

Both k and T<sub>c</sub> should have the same temperature unit, either Kelvin or Celsius.

The curve fitting factor A is used to adjust the I-V characteristics of the cell obtained from (1.1) to give the voltage of a single solar cell which is then multiplied by the number of the cells connected in series to calculate the full array voltage. Since the array current is the sum of the currents flowing through the cells in parallel branches, the cell current  $I_C$  is obtained by dividing the array current by the number of the cells connected in parallel before being used in (1.1), which is only valid for a certain cell operating temperature  $T_c$  with its corresponding solar irradiation level  $S_c$ . If the temperature and solar irradiation levels change, the voltage and current outputs of the PV array will follow this change. Hence, the effects of the changes in temperature and solar irradiation levels should also be included in the final PV array model. A method to include these effects in the PV array modelling is given by Buresch [1]. According to his method, for a known temperature and a known solar irradiation level, a model is obtained and then this model is modified to handle different cases of temperature and irradiation levels. Let (1.1) be the benchmark model for the known operating temperature  $T_c$  and known solar irradiation level  $S_c$  as given in the specification. When the ambient temperature and irradiation levels change, the cell operating temperature also changes, resulting in a new output voltage and a new photocurrent value. The solar cell operating temperature varies as a function of solar irradiation level and ambient temperature. The variable ambient temperature  $T_a$  affects the cell output voltage and cell photocurrent. These effects are represented in the model by the temperature coefficients  $C_{TV}$  and  $C_{TI}$  for cell output voltage and cell photocurrent, respectively, as:

$$C_{TV} = 1 + \beta_T (T_a - T_x) \quad 1.2$$

$$C_{TI} = 1 + \frac{\gamma_T}{S_c} (T_x - T_a) \quad 1.3$$

Where,  $\beta_T = 0.004$  and  $\gamma_T = 0.06$  for the cell used and  $T_a = 20^\circ\text{C}$  is the ambient

temperature during the cell testing. This is used to obtain the modified model of the cell for another ambient temperature  $T_x$ . Even if the ambient temperature does not change significantly during the daytime, the solar irradiation level changes depending on the amount of sunlight and clouds. A change in solar irradiation level causes a change in the cell photocurrent and operating temperature, which in turn affects the cell output voltage. If the solar irradiation level increases from  $S_{x1}$  to  $S_{x2}$ , the cell operating temperature and the photocurrent will also increase from  $T_{x1}$  to  $T_{x2}$  and from  $I_{ph1}$  to  $I_{ph2}$ , respectively. Thus the change in the operating temperature and in the photocurrent due to variation in the solar irradiation level can be expressed via two constants,  $C_{SV}$  and  $C_{SI}$ , which are the correction factors for changes in cell output voltage  $V_C$  and photocurrent  $I_{ph}$ , respectively:

$$C_{SV} = 1 + \beta_T \alpha_S (S_x - S_c) \quad 1.4$$

$$C_{SI} = 1 + \frac{1}{S_c} (S_x - S_c) \quad 1.5$$

where  $S_c$  is the benchmark reference solar irradiation level during the cell testing to obtain the modified cell model.  $S_x$  is the new level of the solar irradiation. The temperature change  $\Delta T_C$ , occurs due to the change in the solar irradiation level and is obtained using

$$\Delta T_C = \alpha_S (S_x - S_c) \quad 1.6$$

The constant  $\alpha_S$  represents the slope of the change in the cell operating temperature due to a change in the solar irradiation level [1] and is equal to 0.2 for the solar cells used. Using correction factors  $C_{TV}$ ,  $C_{TI}$ ,  $C_{SV}$  and  $C_{SI}$ , the new values of the cell output voltage  $V_{CX}$  and photocurrent  $I_{phx}$  are obtained for the new temperature  $T_x$  and solar irradiation  $S_x$  as follows:

$$V_{CX} = C_{TV} C_{SV} V_C \quad 1.7$$

$$I_{phx} = C_{TI} C_{SI} I_{ph} \quad 1.8$$

$V_C$  and  $I_{ph}$  are the benchmark reference cell output voltage and reference cell photocurrent, respectively. The resulting I-V

and P-V curves for various temperature and solar irradiation levels were discussed and shown in [6, 8, 9], therefore they are not going to be given here again.

A general block diagram of the PVA model for GUI environment of Simulink is given in Fig. 2 along with filter and load models. The block called *PVA model for GUI* is the last stage of the model. This block contains the sub models that are connected to build the final model. A diode (D1) is connected in series with the load circuit to prevent the reverse current flow. A filter may be connected before the load to maintain a stable voltage. The PVA consists of 200 PV cells all connected in series to have a desired voltage output. Depending on the load power required, the number of parallel branches can be increased to 2 or more. The effects of the temperature and

solar irradiation levels are represented by two variables gains. Since the main objective is the development of the PVA functional model for the Simulink environment, the other parts of the operational block diagram given in Fig. 2 are not going to be explained in full detail. However, just to describe the main diagram, as it can readily be seen, the system is modeled to supply power to both dc and ac loads. The dc load is directly coupled while the ac load can be fed through a three-phase inverter and an isolation transformer with a turn ratio 1. The last stage of the PVA model is shown in Fig. 2. The other stages are masked as subsystems under the last stage. The mathematical model of a single PV cell given by (1.1) is represented with the block called *Equation 1*.

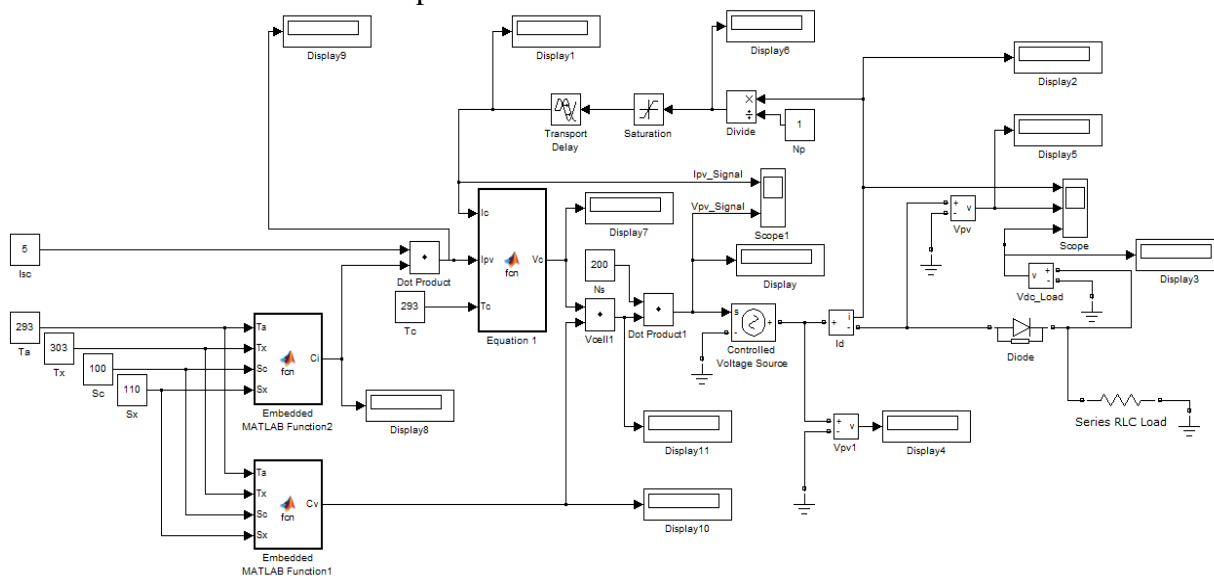


Fig. 2 Solar PV Array Simulated in MATLAB

## 1.2 MODELLING AND SIMULATION OF WTDFIG

The wind turbine and the doubly-fed induction generator (WTDFIG) are shown in the figure called The Wind Turbine and the Doubly-Fed Induction Generator System. The AC/DC/AC converter is divided into two components: the rotor-side converter ( $C_{rotor}$ ) and the grid-side converter ( $C_{grid}$ ).  $C_{rotor}$  and  $C_{grid}$  are Voltage-Sourced Converters that use

forced-commutated power electronic devices (IGBTs) to synthesize an AC voltage from a DC voltage source. A capacitor connected on the DC side acts as the DC voltage source. A coupling inductor  $L$  is used to connect  $C_{grid}$  to the grid. The three-phase rotor winding is connected to  $C_{rotor}$  by slip rings and brushes and the three-phase stator winding is directly connected to the grid. The power captured by the wind turbine is

converted into electrical power by the induction generator and it is transmitted to the grid by the stator and the rotor windings. The control system generates the pitch angle command and the voltage command signals  $V_r$  and  $V_{gc}$  for  $C_{rotor}$  and  $C_{grid}$  respectively in order to control the power of the wind turbine, the DC bus voltage and the reactive power or the voltage at the grid terminals.

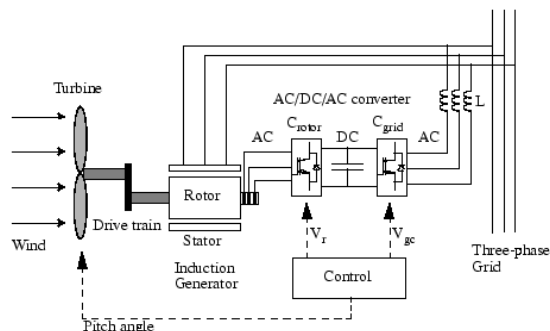


Fig. 3 The Wind Turbine and the Doubly-Fed Induction Generator System

In this figure the followings parameters are used:

$P_m$  Mechanical power captured by the wind turbine and transmitted to the rotor

$P_s$  Stator electrical power output

$P_r$  Rotor electrical power output

$P_{gc}$   $C_{grid}$  electrical power output

$Q_s$  Stator reactive power output

$Q_r$  Rotor reactive power output

$Q_{gc}$   $C_{grid}$  reactive power output

$T_m$  Mechanical torque applied to rotor

$T_{em}$  Electromagnetic torque applied to the rotor by the generator

$\omega_r$  Rotational speed of rotor

$\omega_s$  Rotational speed of the magnetic flux in the air-gap of the generator, this speed is named synchronous speed. It is proportional to the frequency of the grid voltage and to the number of generator poles.

### J Combined rotor and wind turbine inertia coefficient

The mechanical power and the stator electric power output are computed as follows:

$$P_m = T_m \omega_r \quad 1.9$$

$$P_s = T_{em} \omega_s \quad 1.10$$

For a lossless generator the mechanical equation is:

$$J \frac{d\omega_r}{dt} = T_m - T_{em} \quad 1.11$$

In steady-state at fixed speed for a lossless generator  $T_m = T_{em}$  and  $P_m = P_s + P_r$ .

It follows that:

$$P_r = P_m - P_s = T_m \omega_r - T_{em} \omega_s = -T_m \frac{\omega_s - \omega_r}{\omega_s} \omega_s = -s T_m \omega_s = -s P_s,$$

where  $s$  is defined as the slip of the generator:  $s = (\omega_s - \omega_r) / \omega_s$ .

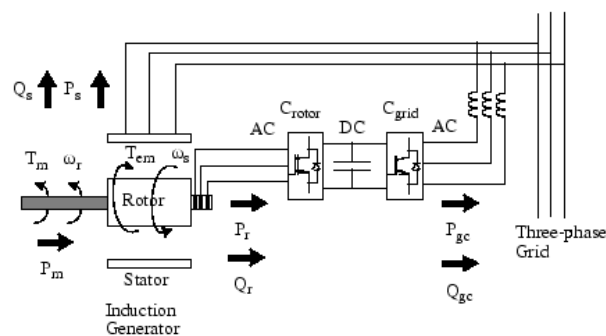


Fig. 4 Power Flow Diagram

Generally the absolute value of slip is much lower than 1 and, consequently,  $P_r$  is only a fraction of  $P_s$ . Since  $T_m$  is positive for power generation and since  $\omega_s$  is positive and constant for a constant frequency grid voltage, the sign of  $P_r$  is a function of the slip sign.  $P_r$  is positive for negative slip (speed greater than synchronous speed) and it is negative for positive slip (speed lower than synchronous speed). For super-synchronous speed operation,  $P_r$  is transmitted to DC bus capacitor and tends to rise the DC voltage. For sub-synchronous speed operation,  $P_r$  is taken out of DC bus capacitor and tends to decrease the DC voltage.  $C_{grid}$  is used to generate or absorb the power  $P_{gc}$  in order to keep the DC voltage constant. In steady-

state for a lossless AC/DC/AC converter  $P_{gc}$  is equal to  $P_r$  and the speed of the wind turbine is determined by the power  $P_r$  absorbed or generated by  $C_{rotor}$ . The power control will be explained below.

The phase-sequence of the AC voltage generated by  $C_{rotor}$  is positive for sub-synchronous speed and negative for super-synchronous speed. The frequency of this voltage is equal to the product of the grid

frequency and the absolute value of the slip.

$C_{rotor}$  and  $C_{grid}$  have the capability of generating or absorbing reactive power and could be used to control the reactive power or the voltage at the grid terminals.

The equations 1.9 to 1.11 and the basic diagrams of Fig. 3 & 4 is used to develop the WTDFIG model in MATLAB, shown if Fig. 5.

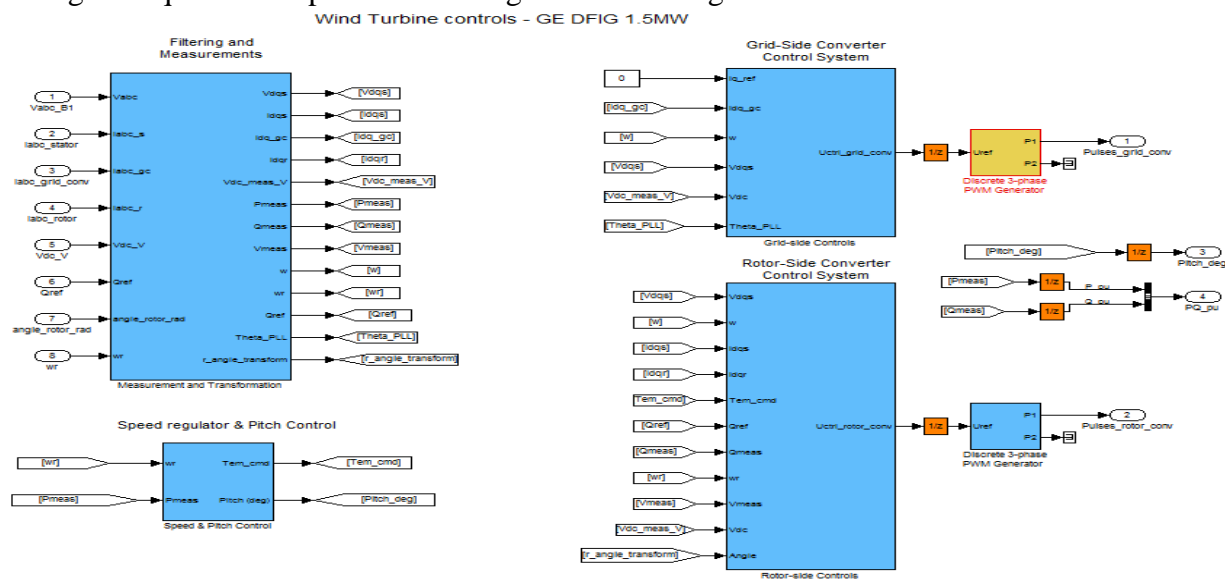


Fig. 5 Detailed WTDFIG model simulated in MATLAB

**Some of the simulation considerations are as follows:**

**WTDFIG modeled using positive-sequence only**

The WTDFIG is modeled by a three-wire system using two current sources. The WTDFIG does not generate any zero-sequence current, but it can generate negative-sequence currents during unbalanced system operation.

**Nominal power, line-to-line voltage and frequency**

The nominal power in VA, the nominal line-to-line voltage in Vrms and the nominal system frequency in hertz.

**Stator [Rs, Lls]**

The stator resistance  $R_s$  and leakage inductance  $L_{ls}$  in pu based on the generator rating.

**Rotor [Rr', Llr']**

The rotor resistance  $R_{r'}$  and leakage

inductance  $L_{lr'}$ , both referred to the stator, in pu based on the generator rating.

**Magnetizing inductance  $L_m$**

The magnetizing inductance  $L_m$  in pu based on the generator rating.

**Inertia constant, friction factor and pairs of poles**

Combined generator and turbine inertia constant  $H$  in seconds, combined viscous friction factor  $F$  in pu based on the generator rating and number of pole pairs  $p$ .

You may need to use your own turbine model, in order for example, to implement different power characteristics or to implement the shaft stiffness. Your model must then output the mechanical torque applied to the generator shaft. If the inertia and the friction factor of the turbine are implemented inside the turbine model you specify only the generator inertia constant

H and the generator friction factor F.

### Initial conditions

The initial slip  $s$ , electrical angle  $\Theta$  in degrees, stator phasor current magnitude in pu, stator phasor current phase angle in degrees, rotor phasor current magnitude in pu and rotor phasor current phase angle in degrees.

### Converter maximum power

The maximum power of both  $C_{grid}$  and  $C_{rotor}$  in pu of the nominal power. This parameter is used to compute the maximum current at 1 pu of voltage for  $C_{grid}$ . The maximum current for  $C_{rotor}$  is 1 pu.

### Grid-side coupling inductor [L R]

The coupling inductance L and its resistance R in pu based on the generator rating.

### Coupling inductor initial currents

The coupling inductor initial phasor current in positive-sequence. The initial value of the current corresponding to the WTDFIG operating point may be specified in order to start simulation in steady state. The system will reach steady-state after a short transient.

### Nominal DC bus voltage

The nominal DC bus voltage in volts.

### DC bus capacitor

The total capacitance of the DC link in farads. This capacitance value is related to the WTDFIG rating and to the DC link nominal voltage. The energy stored in the capacitance (in joules) divided by the WTDFIG rating (in VA) is a time duration which is usually a fraction of a cycle at nominal frequency. For example, for the default parameters, ( $C=10000 \mu\text{F}$ ,  $V_{dc}=1200 \text{ V}$ ,  $P_n=1.67 \text{ MVA}$ ) this ratio  $1/2 \cdot C \cdot V_{dc}^2 / P_n$  is 4.3 ms, which represents 0.26 cycle for a 60 Hz frequency. If you change the default values of the nominal power rating and DC voltage, you should change the capacitance value accordingly.

## 2. AN INTEGRATED HYBRID POWER SYSTEM BASED ON RENEWABLE ENERGY SOURCES

The integrated model of SPA and WTDFIG has been developed and run using MATLAB (version R2011a). The model is as shown in the following figure. The integrated model is run for the data of city Basrah, Iraq. The results will be explained in the next section.

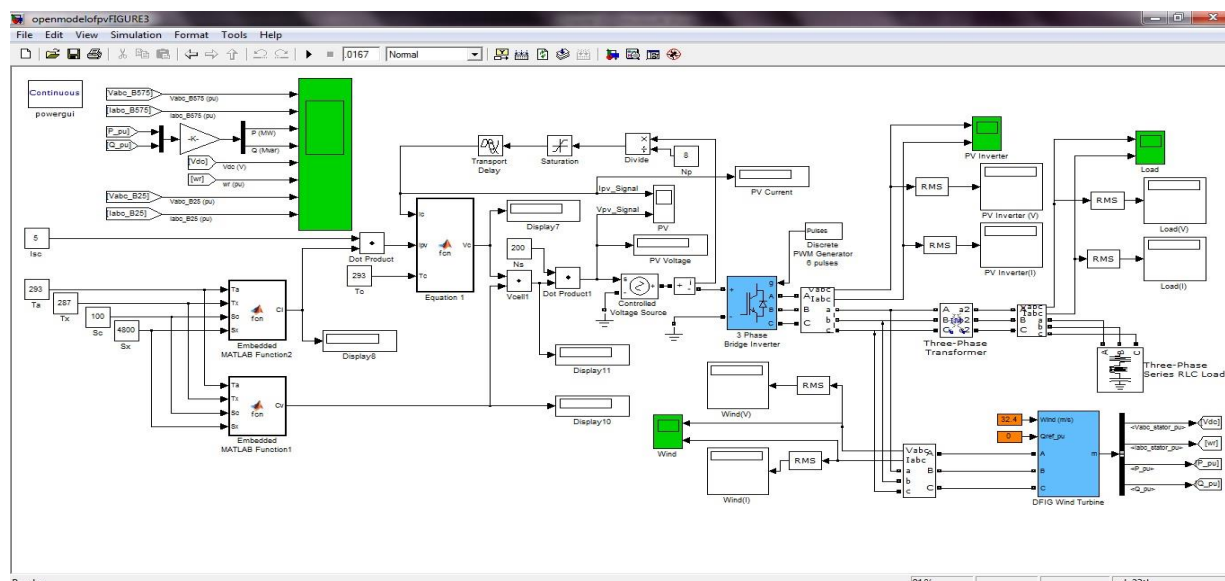


Fig. 6 The integrated system supplying to a common load

## 3. SIMULATION RESULTS

The models are run as standalone models. The results, thus, obtained are just checked

and verified by the theoretical basic equations. The main results are obtained by the integrated power system model of SPA and WTDFIG for the monthly average meteorological data corresponding to the city of Basrah, Iraq.

### 3.1 RESULTS OF SPA STANDALONE MODEL

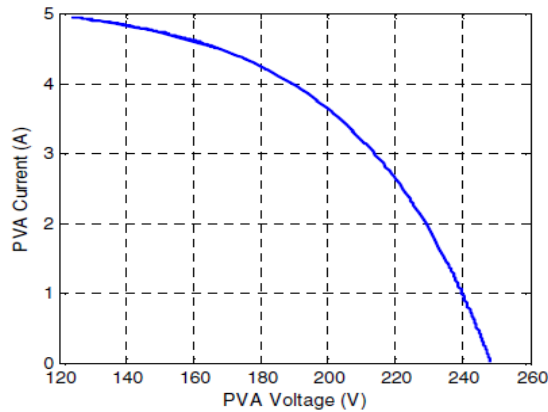


Fig. 7 V-I characteristics of SPA

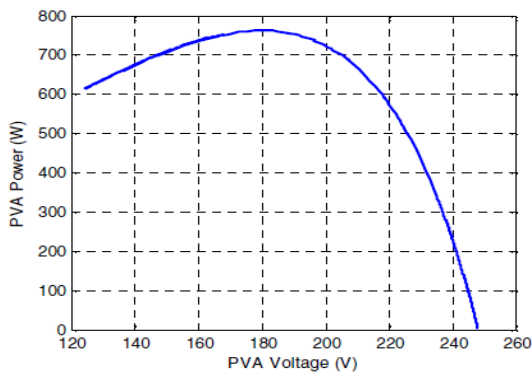


Fig. 8 P-V Characteristics of SPA

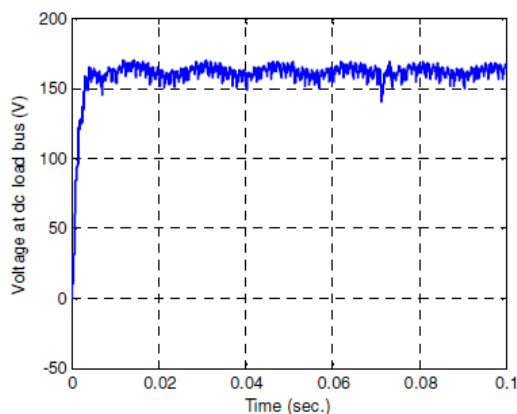


Fig. 9 Voltage at DC load bus

All the results shown above are meeting the requirements of theoretical modelling

based on the design equations.

### 3.2 RESULTS OF WTDFIG STANDALONE MODEL

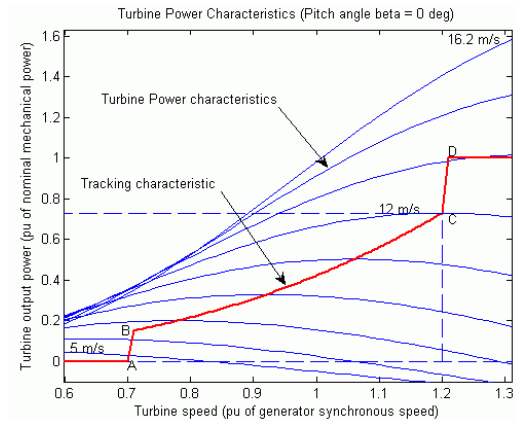


Fig. 10 Turbine Characteristics and Tracking Characteristic

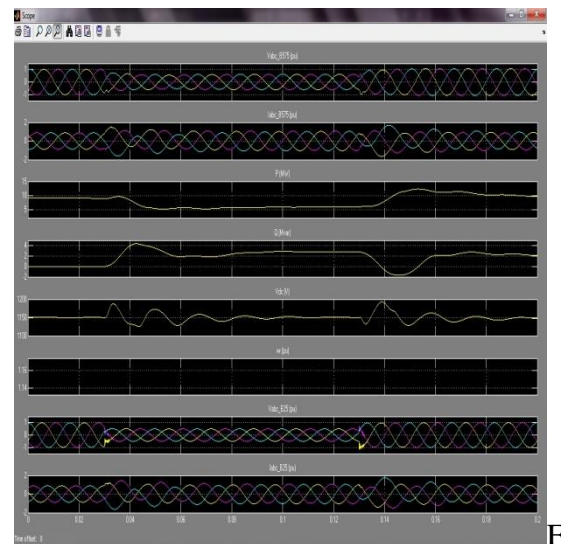


Fig. 11 Results of WTDFIG standalone model for wind speed of 15m/s

### 3.3 RESULTS OF INTEGRATED MODEL OF SPA AND WTDFIG

An Integrated Hybrid Power System Based on Renewable Energy Sources has been developed as discussed in Chapter IV. The hybrid power system consists of a simulated solar PV model and a wind turbine doubly fed induction generator. The isolating transformers are used for the purpose of integration and reduction of circulating currents. The model has been

run for the monthly average data of solar irradiance, temperature and wind speed available for the city of Basrah, Iraq. Table 1 shows the above said data. The data has been taken from the official websites for the purpose of simulation alone. Source: [http://www1.eere.energy.gov/windandhydro/wind\\_how.html](http://www1.eere.energy.gov/windandhydro/wind_how.html) and <http://www.weatherbase.com>

	Temp K	Solar w/m <sup>2</sup>	Wind Speed m/s
January	285	5000	43.2
February	288	6000	43.2
March	293	6200	57.6
April	298	6100	43.2
May	303	6400	57.6
June	306	6500	72
July	308	6200	68.4
August	307	6900	61.2
September	305	7000	50.4
October	300	6100	50.4
November	293	5500	43.2
December	287	4800	32.4

1 shows the above said data. The data has been taken from the official websites for the purpose of simulation alone. Source:

[http://www1.eere.energy.gov/windandhydro/wind\\_how.html](http://www1.eere.energy.gov/windandhydro/wind_how.html) and <http://www.weatherbase.com>

The results corresponding to the average monthly data of Basrah, Iraq is shown in Table 2

The graphical representation of the results of hybrid power system model is shown below:

**Table 2 The simulation results for power output of SPA, WTDFIG and at load.**

	PV output				Wind output			
	Voltage Volt	Current Amp	Power Watt	Power MW	Voltage Volt	Current Amp	Power Watt	Power MW
January	250	1.73E+04	4.33E+06	<b>4.33</b>	250	1.73E+04	4.32E+06	<b>4.32</b>
February	291.6	1.99E+04	5.80E+06	<b>5.80</b>	291.6	1.92E+04	5.60E+06	<b>5.60</b>
March	294.5	2.01E+04	5.91E+06	<b>5.91</b>	294.5	1.94E+04	5.70E+06	<b>5.70</b>
April	284.5	1.96E+04	5.56E+06	<b>5.56</b>	284.5	1.89E+04	5.37E+06	<b>5.37</b>
May	291	1.99E+04	5.79E+06	<b>5.79</b>	291	1.92E+04	5.58E+06	<b>5.58</b>
June	291.4	1.99E+04	5.81E+06	<b>5.81</b>	291.4	1.93E+04	5.61E+06	<b>5.61</b>
July	276.8	1.93E+04	5.33E+06	<b>5.33</b>	276.8	1.86E+04	5.15E+06	<b>5.15</b>
August	306.4	2.10E+04	6.43E+06	<b>6.43</b>	306.4	2.02E+04	6.20E+06	<b>6.20</b>
September	313.1	2.11E+04	6.60E+06	<b>6.60</b>	313.1	2.04E+04	6.37E+06	<b>6.37</b>
October	281.9	1.94E+04	5.48E+06	<b>5.48</b>	281.9	1.88E+04	5.29E+06	<b>5.29</b>
November	264.3	1.86E+04	4.92E+06	<b>4.92</b>	264.3	1.80E+04	4.75E+06	<b>4.75</b>
December	239.9	1.74E+04	4.16E+06	<b>4.16</b>	239.9	1.67E+04	4.00E+06	<b>4.00</b>

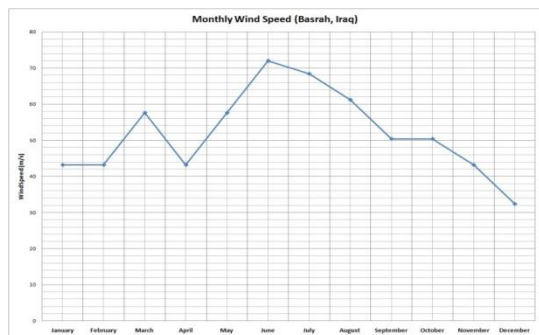


Fig. 12 Average monthly wind speed of Basrah, Iraq in m/s

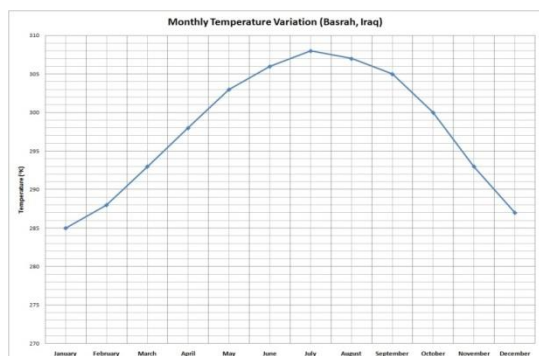


Fig. 13 Average monthly temperature of Basrah, Iraq in °K

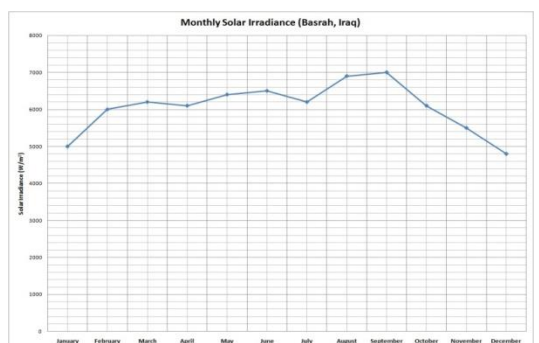


Fig. 14 Average monthly Solar Irradiance of Basrah, Iraq in  $W/m^2$

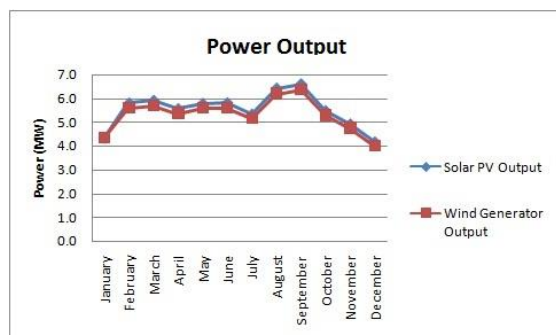


Fig. 15 Results of Hybrid Power System consists of SPA and WTDFIG

## 4 CONCLUSIONS AND FUTURE SCOPE

From the above results it is clear that the SPA and WTDFIG is running in synchronism and is able to feed power to standalone loads or to the grid. It is seen from the results that the plant output is maximum, around 13MW, in the month of September and minimum in December, around 8MW. This is due to the fact that the solar and wind both are having highest and lowest values in the month of September and December, respectively. The monthly variation shown here does not depict the daily variation in solar or wind parameters. The solar PV array model is designed for supplying 8MW power and the wind turbine doubly fed induction generator is designed for supplying 9MW power. As an integrated hybrid model the power system is capable of supplying 17MW maximum power. The average power supplied by the hybrid model will be somewhere 10MW. Additional 5MW can be added if the Biogas Plant will also be added to this model. This model is made and results are obtained corresponding to the data available for the city of Basrah, Iraq. The model is useful not only for this city but for any city.

In future, the biogas plant can also be modeled and made to integrate along with solar and wind. This model of integrated power system gives us an idea of replacement of conventional energy sources which is very important in the countries like Iraq. Similar case studies may be made for other cities to develop the integrated models of renewable energy sources.

## 5. REFERENCES

- [1]. M. Buresch: *Photovoltaic Energy Systems Design and Installation*, McGraw-Hill, New York, 1983.
- [2]. Z. M. Salameh and F. Dagher: *The effect of electrical array reconfiguration on the performance of a PV powered volumetric*

water pump, IEEE Trans., EC-5 (1990) 653-658.

[3]. J. A. Roger: *Theory of the direct coupling between DC motors and photovoltaic solar arrays*, Solar Energy, 23 (1979) 193-198.

[4]. W. Z. Faro and M. K. Balaehander: *Dynamic performance of a DC shunt motor connected to a photovoltaic array*, IEEE Trans., EC-3 (1988) 613-617.

[5]. J. Appelbaum: *Starting and steady-state characteristics of DC motors powered by solar cell generators*, IEEE Trans., EC-1 (1986) 17-25.

[6]. I. H. Altas and A. M. Sharaf: *A solar powered permanent magnet DC motor drive scheme*, Proc. 17th Annu. Conf. Solar Energy Soc. Canada, Toronto, Ont., Canada, 19.91, pp. 65-71).

[7]. A. M. Sharaf and L. Wang: *A photovoltaic powered efficient DC motor drive for pump irrigation*, Proc. Canad. Solar Energy Conf., Halifax, N.S., Canada, 1990.

[8]. I. H. Altas and A. M. Sharaf: *A Fuzzy Logic Power Tracking Controller For A Photovoltaic Energy Conversion Scheme*, Electric Power Systems Research Journal, Vol.25, No.3, pp.227-238, 1992.

[9]. I. H. Altas and A.M. Sharaf: *A Novel On-Line MPP Search Algorithm For PV Arrays*, IEEE Transactions on Energy Conversion, Vol. 11, No. 4, December 1996, pp. 748-754.

[10]. M.A.S Masoum, And H. Dehbonei: *Design, Construction and Testing of a Voltage-based Maximum Power Point Tracker (VMPPT) for Small Satellite Power Supply*, 13th Annual AIAA/USU Conference on Small Satellites, pp.1-12., 1999.

[11]. Y-C. Kuo, T-J. Liang, and J-F. Chen: *Novel Maximum-Power-Point-Tracking Controller for Photovoltaic Energy Conversion System*, IEEE Transactions On Industrial Electronics, Vol. 48, No. 3, June 2001, Pp.594-601.

[12]. T. Noguchi, S. Togashi, and R. Nakamoto: *Short-Current Pulse-Based Maximum-Power-Point Tracking Method for Multiple Photovoltaic and Converter Module System*, IEEE Transactions on Industrial Electronics, Vol. 49, No. 1, February 2002, 217-223.

[13]. M. A. S. Masoum, H. Dehbonei, and E. F. Fuchs: *Theoretical and Experimental Analyses of Photovoltaic Systems with Voltage- and Current-Based Maximum Power-Point Tracking*, IEEE Transactions On Energy Conversion, Vol. 17, No. 4, December 2002, Pp.514-522.

[14]. Hua and J. Lin: *An on-line MPPT algorithm for rapidly changing illuminations of solar arrays*, Renewable Energy 28 (2003) 1129-1142.

[15]. K. Benlarbi, L. Mokrani, M.S. Nait-Said: *A fuzzy global efficiency optimization of a photovoltaic water pumping system*, Solar Energy, 77 (2004) 203-216.

[16]. Hua and J. Lin: *A modified tracking algorithm for maximum power tracking of solar array*, Energy Conversion and Management, 45 (2004) 911-925.

[17]. Y-M. Chen, Y-C. Liu, and F-Y. Wu: *Multiinput Converter With Power Factor Correction, Maximum Power Point Tracking, and Ripple-Free Input Currents*, IEEE Transactions On Power Electronics, Vol. 19, No. 3, May 2004, pp.631-639.

[18]. Matlab and Simulink, The Mathworks, Inc. as of September 2006, <http://www.mathworks.com>.

[19]. R. Pena, J.C. Clare, G.M. Asher, "Doubly fed induction generator using back-to-back PWM converters and its application to variable-speed wind-energy generation," IEEE Proc.-Electr. Power Appl., Vol. 143, No. 3, May 1996

[20]. Vladislav Akhmatov, "Variable-Speed Wind Turbines with Doubly-Fed Induction Generators, Part I: Modelling in Dynamic Simulation Tools," Wind Engineering Volume 26, No. 2, 2002

[21]. Nicholas W. Miller, Juan J. Sanchez-Gasca, William W. Price, Robert W. Delmerico, "DYNAMIC MODELING OF GE 1.5 AND 3.6 MW WIND TURBINE-GENERATORS FOR STABILITY SIMULATIONS," GE Power Systems Energy Consulting, IEEE WTG Modeling Panel, Session July 2003